JOURNAL OF THERMOPHYSICS AND HEAT TRANSFER
Vol. 26, No. 2, April–June 2012

Turbulent Radiation Statistics of Exhaust Plumes Exiting from a Subsonic Axisymmetric Nozzle

David Blunck,* Matthew Harvazinski, Brent Rankin, Charles Merkle, and Jay Gore
Purdue University, West Lafayette, Indiana 47907

DOI: 10.2514/1.T3621

Improved understanding of radiation emissions from exhaust plumes are needed for safety applications. Relevant literature has focused on characterizing mean radiation properties of exhaust plumes. Turbulent radiation properties reported for flames have been used to provide insight into scalar distribution within the flows, improve understanding of turbulence radiation interactions, and estimate integral time and length scales. Motivated by this, radiation intensity measurements of subsonic exhaust plumes were acquired using a high-speed infrared camera (up to 11,300 Hz). The mean, root mean square, probability density function, auto and spatial correlation coefficients, integral time and length scales, and power spectral density functions of the measured radiation intensity are reported near the tip of the potential core and downstream. Axial and radial variation in radiation intensity fluctuations is similar to those reported for flames. Autocorrelation coefficients of the radiation intensity are approximated reasonably well by exponential curves. Integral time and length scales increase monotonically downstream of the core region and are consistent with Taylor's hypothesis. The break frequency and slope of the normalized power spectral density function are comparable to those reported for turbulent jet flames. These findings suggest that reacting flows can be used to predict trends in turbulent radiation properties of exhaust plumes.

Nomenclature

c	=	speed of sound, m/s
D	=	nozzle exit diameter, m
$E(f)$	=	power spectral density function
f	=	frequency, 1/s
$I_{\Delta\lambda}$	=	spectrally integrated intensity, W/m^2-sr
l	=	integral length scale, m
Ma	=	Mach number
$\dot{m}_a$	=	air mass flow rate, kg/s
N	=	number of measurements in sample
r	=	radial distance, m
Re	=	Reynolds number
s	=	radial or axial location, m
T_e	=	temperature at nozzle exit, K
T_n	=	temperature inside nozzle, K
t	=	time, s
u	=	velocity in axial direction, m/s
w	=	width of probability density function bin
X	=	mole fraction
z	=	axial distance
Γ	=	Fourier transform
μ	=	dynamic viscosity, N s/m^2
ρ	=	density, kg/m^3
$\rho(\Delta s)$	=	spatial correlation coefficients
$\rho(\Delta t)$	=	autocorrelation coefficients
τ	=	integral time scales, s
Φ	=	equivalence ratio

Subscripts

0	=	nozzle exit
b	=	bin
CO_2	=	carbon dioxide
H_2O	=	water vapor
i	=	individual measurement
max	=	maximum value
mean	=	mean value
min	=	minimum value
n	=	measurement in nozzle
r	=	radial direction
z	=	axial direction

Received 7 September 2010; revision received 7 November 2011; accepted for publication 12 November 2011.

*School of Mechanical Engineering; Currently, Propulsion Directorate, Combustion Branch, U.S. Air Force Research Laboratory, Wright–Patterson AFB, Ohio.

†School of Mechanical Engineering.

Introduction

IMPROVED understanding of radiation emissions from exhaust plumes is needed for safety applications [1]. Relevant literature typically has compared mean radiation emissions from plumes for a range of nozzle geometries and exit conditions. Banken et al. [2] generally observed little variation in the mean radiant power emitted from plumes exiting from axisymmetric and wedge nozzles. Ajdari et al. [3] used time-averaged spectrally integrated radiation intensity measurements of plumes to show that sonic flows have enhanced afterburning compared with supersonic flows. This results from enhanced mixing and stronger shock structures at the nozzle exit for sonic flows. Sugiyama et al. [4] provided time-resolved infrared images and mean radiant power measurements of plumes exiting from rectangular nozzles. Increasing the nozzle aspect ratio typically reduced the radiant power emitted from the plume. Heragu et al. [5] and Decher [6] calculated the radiation intensity and radiant power emitted from the potential core region of plumes. Radiation emissions were characterized for a range of operating conditions. Knowles and Saddington [7] suggested that reducing the size of the potential core is important for reducing the infrared signature of exhaust plumes. Mahulikar et al. [1] calculated the spectral radiation intensity of a plume after 5 km of atmospheric absorption. The majority of the radiation emitted from a plume is absorbed by the atmosphere over that distance except for radiation in the 4.15–4.2 μm spectral band.

The turbulent nature of radiation emissions from exhaust plumes has been reported in several studies. Adjari et al. [3] found that time-dependent radiation intensity measurements were up to a factor of 5 larger than average values for weakly afterburning plumes. Pearce and Varma [8] calculated the spectrally integrated radiation intensity emitted from afterburning missile plumes using mean and fluctuating scalar values. The mean intensity increased by up to a factor of 2.5

toward the edges of the plume (where less afterburning occurred) when turbulent fluctuations were considered. Calhoon and Kenzakowski [9] used a probably density function method to account for turbulence-chemistry interactions in an afterburning missile plume. Turbulence-chemistry interactions had a strong effect on the infrared signature of the plumes as afterburning approached shutdown. Blunck et al. [10] reported the mean, root mean square, probably density function, skewness, and kurtosis of the radiation intensity along lines of sight through the centerline of exhaust plumes. The former three statistics were used for verifying time-dependent and mean calculated intensity values.

Radiation intensity measurements provide a nonintrusive technique for studying turbulent flows. The combustion community has used turbulent radiation statistics to understand the importance of turbulence radiation interactions in flames [11,12], distinguish combusting flows from background radiation [13,14], and estimate integral time and length scales [15,16]. Similar insights can be gained by studying turbulent radiation properties in nonreacting exhaust plumes. Turbulent statistics reported for radiation intensity or mixture fraction measurements of flames have included the root mean square [13,15], probability density functions [11,12], skewness [17], auto and spatial correlation coefficients [18,19], integral time scales [11], and power spectral density functions [11,17,20]. The typical Reynolds numbers of flames where turbulent statistics have been reported are 3000–33,600 [11,13,15,18,20].

Turbulent radiation statistics of flames can be used for comparison to exhaust plumes. Zheng et al. [15] reported radial profiles of the root mean square of the spectral radiation intensity normalized by mean values for partially premixed flames. The normalized root mean square of the radiation intensity was nearly constant for the line-of-sight measurements through the central portion of the flame, but increased by a factor of 1.5 or more toward the edges. Kounalakis et al. [14] reported that probably density functions of spectral intensity measurements of jet flames became skewed toward negative values downstream in the flow. Zheng and Gore [20] noted that the skewness of probability density functions of the radiation intensity increased with radial distance in jet flames. The increased skewness, both downstream and radially, resulted from a greater prevalence of hot and cold pockets of radiating species along lines of sight through the flow. Kounalakis et al. [11] found that auto and spatial correlation coefficients of mixture fraction fluctuations in diffusion flames are approximated reasonably well by an exponential decay after scaling with respect to the integral time or length scale. Using this scaling, Dylla et al. [18] found reasonable agreement between an exponential decay and auto and spatial correlation coefficients of the measured radiation intensity emitted from small volumes within a luminous jet flame. At some axial and radial locations the correlations undershot below zero. Kounalakis et al. [11] reported that integral time and length scales of radiation intensity increased with distance downstream in jet flames. Zheng et al. [16] used a deconvolution technique to show that the integral time and length scales within a jet flame increase by a factor of 2 or more between the centerline and edges of the flow. Kounalakis et al. [11] found that the power spectral density function of mixture fraction fluctuations in nonluminous flames was independent of axial location through proper scaling. Slopes near $-5/3$ and $-5/2$ have been reported for the inertial-like subrange of power spectral density functions of radiation intensity measurements of hydrogen/air [14] and ethylene/air [20] flames, respectively. Silva et al. [17] reported a slope of $-5/2$ for isotropic turbulent radiation intensity calculations.

Given this review of the relevant literature, the objectives of this work are as follows:

1) Measure the radiation intensity emitted from exhaust plumes using a high-speed infrared camera.

2) Determine the mean, root mean square, probability density function, auto and spatial correlation coefficients, integral time and length scales, and power spectral density functions of the radiation intensity.

3) Compare turbulent radiation properties of plumes to those reported for flames.

The key contributions of this work to the literature are twofold. First, insight is provided into the turbulent nature of radiation emissions from exhaust plumes. Second, turbulent radiation statistics are contrasted between high Reynolds number (e.g., $>200,000$) exhaust plumes and low Reynolds number reacting flow (e.g., $<30,000$) for the first time.

Experimental Approach

Plume Generation

Figure 1 illustrates the experimental arrangement used for generating exhaust plumes and acquiring radiation intensity measurements. This arrangement has been reported previously [21] and is summarized for reader convenience. High-pressure dry air was supplied to a gas turbine combustor can mounted in a pressure vessel. The air was nominally heated to a temperature of 440 ± 15 K. The operating fuel (Jet A) fuel was injected into the air stream through an atomizer. The fuel and air reacted in the combustor to form hot combustion products. A perforated plate, placed downstream of the combustor, was used to pressurize the vessel. The holes were drilled at a 10 deg angle, which imparted a slight swirl to the flow. The exhaust flowed from the perforated plate and exited through the (converging) nozzle into the atmosphere. The nozzle was 16 cm long and had inlet and exit diameters of 12.9 and 9.1 cm, respectively. The exit diameter was used for nondimensionalizing axial and radial distances. A layer of insulation ($\sim$9 cm) was applied to the nozzle to reduce heat loss from the exhaust.

Pressure and temperature measurements were acquired along the length of the experimental arrangement and used to determine the operating conditions. Air mass flow rates were determined from temperature and pressure measurements upstream of a choked orifice. The Reynolds number at the nozzle exit was determined using the nozzle exit diameter, the measured air mass flow rate, and the properties of air at the nozzle exit temperature:

$$Re = \frac{\rho u_0 D}{\mu} = \frac{4\dot{m}_a}{\pi D \mu} \tag{1}$$

The fuel flow rate contributed less than 2% of the total mass flow rate. The properties of air were used because 7% or less of the

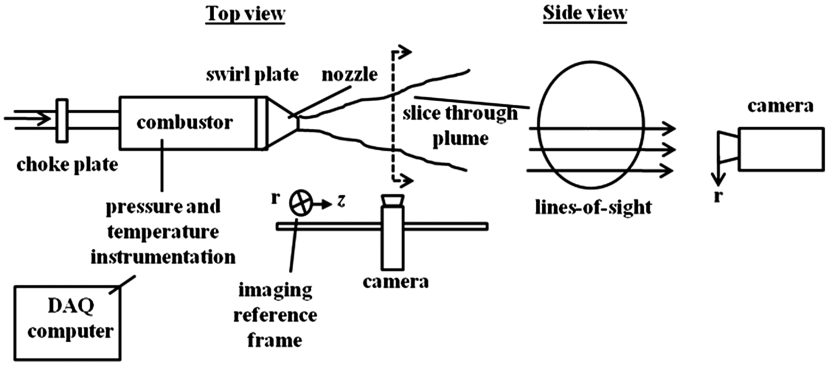

Fig. 1 Experimental arrangement for generating exhaust plumes and obtaining radiation intensity measurements.

calculated exhaust products were carbon dioxide and water vapor. The remainder of the exhaust was primarily air. The temperature of the exhaust was measured upstream of the nozzle at the location where the diameter inside the nozzle was approximately 11.5 cm. Measuring the temperature at this location instead of at the nozzle exit reduced disturbances in the flow at the exit. The nozzle exit temperature was determined from the measured upstream temperature, the Mach number of the flow, and isentropic relationships. The Mach number was determined from the mass flow rate and the fluid properties of air at the nozzle exit conditions:

$$Ma = \frac{u_0}{c} = \frac{4\dot{m}_a}{\pi D^2 \rho c} \tag{2}$$

Fuel mass flow rates were obtained using a factory calibrated turbine flow meter. A portion of the air entering the combustor was used for convective cooling of the combustor liner. Consequently what is reported is a global equivalence ratio. Note that complete combustion products exit the nozzle (i.e., nonreacting) based on comparisons between measured and chemical equilibrium water vapor and carbon dioxide mole fractions [21].

Table 1 lists the average operating conditions of the plumes. The air mass flow rate was fixed during the experiments (0.7 kg/s) while the fuel mass flow rate was varied (5–11 g/s). The equivalence ratio increased by more than a factor of 2 (0.11–0.25), while the Reynolds numbers (230,000–260,000) and Mach numbers (0.4) were nearly constant. Increasing the equivalence ratio increased the temperature and mole fractions of carbon dioxide and water vapor in the plume, as shown in Table 1. The mole fractions were estimated based on chemical equilibrium calculations. Prior comparisons of calculated and measured species concentrations were in reasonable agreement [21].

Radiation Intensity Measurements

Narrowband radiation intensity measurements were acquired using a high-speed infrared camera (up to 11,300 Hz). The camera was mounted perpendicular to the plume axis and moved along a traverse rail as illustrated in Fig. 1. The spatial resolution of the measurements was approximately 3 mm^2. A narrowband filter (4.34 ± 0.1 μm) was used to reduce background radiation and the uncertainty associated with the spectral response of the detector. Primarily radiation emitted from carbon dioxide was acquired in this spectral range. The camera measured the spectrally integrated radiation intensity after attenuation due to the lens, filter, and variations in the spectral response of the detector. Note that the spectral bandwidth of the filter allowed spectrally broadened portions of the radiation intensity to be measured. The intensity was measured along lines of sight through the plume and was reported from an observer's coordinate system, as illustrated in Fig. 1. The axial length is the distance along the centerline from the nozzle exit. The radial length is the distance from the centerline as imaged by the camera [20]. The camera was calibrated by measuring the radiation intensity emitted by a blackbody and correlating this to the reported photon counts. Optical losses and the varying spectral response of the detector were considered during calibration. Note that the distance between the camera and the plume ($\sim$1 m) was such that a portion of radiation intensity was attenuated before reaching the detector. The blackbody was placed the same distance from the camera as the plume centerline to help account for atmospheric absorption. This approach does not compensate for an increase in atmospheric carbon dioxide concentrations in the immediate vicinity of the plume during testing.

Table 1 Dimensional and nondimensional operating conditions for exhaust plumes

Test	Φ	T_n, K	T_0, K [a]	X_{CO_2} [b]	X_{H_2O} [b]	$\dot{m}_a$, kg/s	$Re \times 10^{-5}$	Ma
1	0.11	760	745	0.016	0.015	0.7	2.6	0.4
2	0.19	830	810	0.027	0.026	0.7	2.6	0.4
3	0.25	945	745	0.036	0.034	0.7	2.3	0.4

[a]Based on isentropic relationships.
[b]Chemical equilibrium calculations.

The integration time of the detector was set to between 0.05 and 0.15 ms based on the peak radiation intensity. Adjusting the integration time allowed the full range of the detector to be used. The camera was moved along the traverse rail to allow measurements along the length of the plume. Mean values were averaged where spatial overlap occurred. Seven thousand or more images were obtained of the plume. Measurements were acquired using the entire camera focal plane array to gain spatial information of the turbulent radiation statistics. The sampling frequency was approximately 340 Hz. The root mean square, probability density functions, and spatial correlation coefficients were determined from these measurements. The former two statistics are based on a single line-of-sight (i.e., pixel) through the plume at a given axial or radial location. The axial correlation coefficients were for multiple (adjacent) lines of sight through the centerline. The radial correlation coefficients are for multiple lines of sight starting at the centerline and moving out radially, at a given axial location. Equations for the turbulent statistics are reported in the Appendix. Integral length scales were determined by integrating the area beneath the spatial correlation coefficient until the curve crossed below zero. The temporal resolution of the measurements was increased by sampling only the portion of the focal plane array corresponding to the plume axis. Measurements were obtained at the maximum sampling frequencies; 11,300 and 5300 Hz for integration times of 0.05 and 0.15 ms, respectively. Mean values, autocorrelation coefficients, and power spectral density functions of the radiation intensity (see Appendix for equations) were determined from the high frequency measurements for a given line-of-sight. Integral time scales were determined by integrating the area beneath the autocorrelation coefficient until the curve crossed below zero [18].

Turbulent radiation intensity statistics are reported at two nozzle diameters downstream and beyond. This corresponds to the region near the tip of the potential core and downstream. Close to the nozzle exit, the radiation intensity along lines of sight through the plume is dominated by steady radiation emission from the potential core. The effect of the steady radiation emission on turbulent statistics is evident in the integral time and length scales, which decrease with increasing distance from the nozzle exit in the potential core region. Additional work is required to characterize the combined effect of steady emission from the core and fluctuations in the surrounding shear layer on turbulent radiation properties.

The average uncertainty in the mean radiation intensity is 30% (95% confidence) for values greater than 20% of the peak intensity ($I_{\Delta\lambda,}/I_{\Delta\lambda,\max} > 0.2$). The uncertainty increases to 100% for intensity values less than 20% of the peak value ($I_{\Delta\lambda,}/I_{\Delta\lambda,\max} < 0.2$) [21]. Representative error bars are included in the plot of mean radiation intensity. The uncertainty of the measurements was determined using the approach of Moffat, where a Chi-squared distribution was applied to the measured uncertainty from an auxiliary experiment [22]. Repeated radiation intensity measurements of an exhaust plume were acquired over several days using the same arrangement with representative operating conditions. An auxiliary experiment was used because the large-scale limited repeated measurements for each of the conditions reported in this work.

Results and Discussion

Time-averaged radiation intensity measured for lines of sight through the plume centerline are reported in Fig. 2 for the three operating conditions. The values have been reported and discussed previously [10] and are summarized for completeness of the statistics. The intensity emitted by the plumes decreases with decreasing equivalence ratio, as expected due to lower temperature and radiating species concentrations (see Table 1). The measured axial intensity profiles decay linearly near the nozzle exit and in an exponential manner starting near one diameter downstream [21]. Plots of the radiation intensity normalized by the peak intensity (not shown) nearly collapse for the three equivalence ratios. This is in

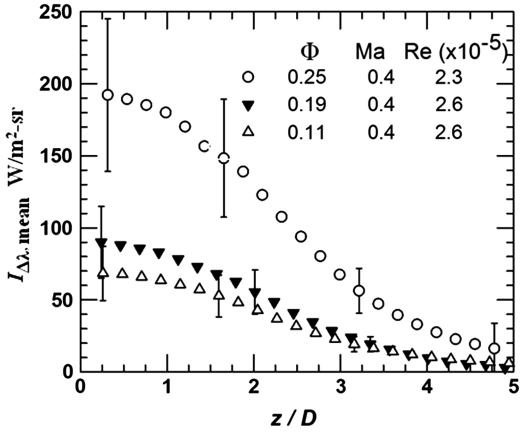

Fig. 2 Average radiation intensity along the centerline of plumes with varying equivalence ratios. The data has been reported previously [10] and is repeated for reader convenience.

agreement with previous work, which indicated that the axial decay in the intensity is typically independent of equivalence ratio [21].

The radiation intensity measured near the nozzle exit is primarily emitted from the potential core. The length of the core was estimated from calculated temperatures for the plume with the highest equivalence ratio (0.25). The temperature was found by solving the full Navier–Stokes equations for a three-dimensional geometry including the nozzle and surrounding air. The boundary conditions and numerical scheme for the calculations were reported by Blunck et al. [10]. The centerline temperature remains constant until approximately two and one-half nozzle diameters downstream beyond which it decays, indicating the end of the potential core. Estimating the core length based on the temperature profile is appropriate due to the nonlinear dependence of radiation on temperature. Temperature measurements in a heated jet of air (∼400 K) with an equivalent Mach number and a Reynolds number of the same order of magnitude (3.8×10^5) indicated a core length between two and three nozzle diameters [21]. Measurements were collected in heated air instead of exhaust to avoid damaging the traverse equipment and are treated as representative. The influence of the constant radiation emitted from the core was evident in the integral time and length scales until one and one-half diameters downstream.

Figure 3 reports the root mean square of the radiation intensity normalized by the mean intensity at two diameters downstream and beyond for the plume with the highest equivalence ratio ($\Phi = 0.25$, $Ma = 0.4$, $Re = 2.3 \times 10^5$). Similar trends were observed for the plumes with smaller equivalence ratios. The normalized root mean square represents the magnitude of the fluctuations in the radiation intensity as a result of variations in the scalar values (i.e., temperature and radiating species mole fractions) along lines of sight. Normalized

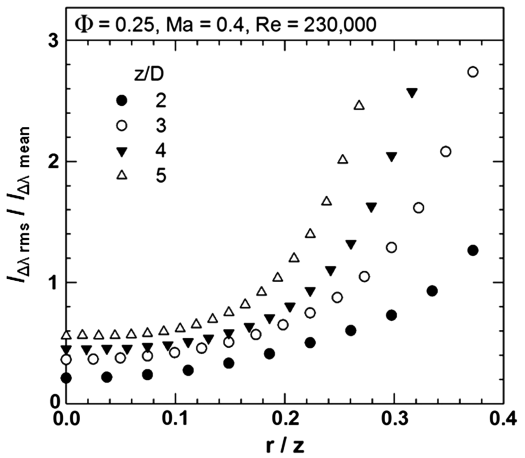

Fig. 3 Normalized root mean square of the radiation intensity at four axial locations for the plume with the highest equivalence ratio.

fluctuations in the radiation intensity emitted from diametric paths increase from 0.2 to 0.55 between two and five diameters downstream. Values between 0.15 and 1.07 have been reported at various axial locations (e.g., z/D of 35, 50, 65) in reacting jet flames ($Re = 3,000$–$33,600$) [11,13,15]. Normalized fluctuations of the radiation intensity increase more rapidly downstream (relative to nozzle or burner diameter) in the plumes than in flames. Increased entrainment and mixing downstream is responsible for the larger reduction in scalar values in plumes. This is in contrast to flames where large scalar values are maintained in the flame sheet. Radial profiles of normalized fluctuations of the radiation intensity are nearly constant until r/z of 0.1 or larger, beyond which the values increase toward the edges of the plume. Similar profiles for the normalized fluctuations have been reported for ethylene, methane, and methane/hydrogen/nitrogen flames [15,16,19]. Intermittent regions of hot and cold carbon dioxide become more prevalent along lines of sight farther downstream and near the edges of the plume and cause the increase in the normalized fluctuations.

Probability density functions of the radiation intensity emitted from the plume with the lowest equivalence ratio (0.11) are reported in Fig. 4. The plumes with higher equivalence ratios (i.e., 0.19 and 0.25) had similar trends and are not reported for brevity. Panels on the left side are line-of-sight measurements through the centerline; panels on the right side are for chordlike paths corresponding to $r/z = 0.25$. Peak values for chordlike paths at four and five diameters downstream are larger than 1.5, and are not shown to allow for trends in the other values to be clear. The probability density functions become skewed toward negative values with increasing axial or radial distance. A greater skewness toward negative values has been reported for increasing radii in flames [19,20]. This results from increasingly intermittent radiation emission toward the outer edges of the flow [20]. Scalar values fluctuate between those of the surroundings and the exhaust plume. A cutoff for low-intensity values is observed for the measurements at $r/z = 0.25$ and three

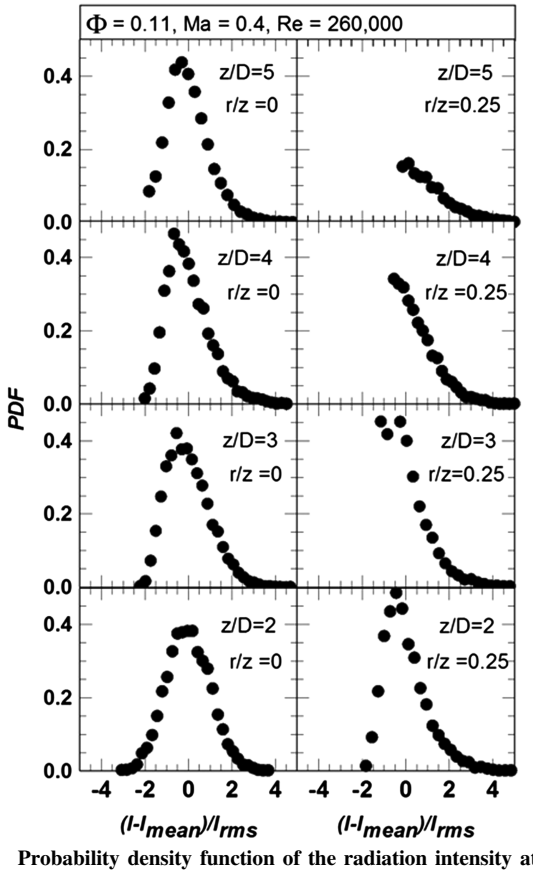

Fig. 4 Probability density function of the radiation intensity at four axial locations along the centerline and at $r/z = 0.25$ for the plume with the lowest equivalence ratio.

diameters downstream and beyond. This occurs because the minimum radiation intensity value is zero.

Figure 5 reports axial and radial spatial correlation coefficients of the radiation intensity emitted from the exhaust plume with the lowest equivalence ratio (0.11). The coefficients are an indication of the degree to which fluctuations in the intensity at two locations are correlated. The location where the correlation tends to zero indicates the maximum distance between which fluctuations in the path integrated intensity are correlated with another line-of-sight. The limited axial correlation coefficients at four diameters downstream are an artifact of the limited camera view for those measurements. Changes in the axial and radial distances are normalized with respect to the integral length scales following the approach of Kounalakis et al. [11]. Exponential decay curves, which have been used in the combustion community to represent spatial correlation coefficients [11,18], provide reasonable agreement with axial and radial correlation coefficients at some downstream locations (e.g., radial $z/D = 2$; axial $z/D = 5$). At the other locations, the exponential profiles overshoot the correlation values. Similarly, Dylla et al. [18] reported good agreement between exponential profiles and radial correlation coefficients of local radiation intensity measurements at some flame locations, and overshooting of the exponential curves at other locations.

Axial and radial integral length scales of the line-of-sight radiation intensity measurements are shown in the top and bottom panels, respectively, of Fig. 6. Integral length scales represent the characteristic size of larger turbulent eddies in the flow [23] and are useful for modeling turbulent intensity fluctuations [15]. The length scales in this work are the path integrated values as a result of the line-of-sight radiation measurements. The integral length scales in the axial and radial directions of the exhaust plume increase monotonically starting near two diameters downstream. An increase in length scales

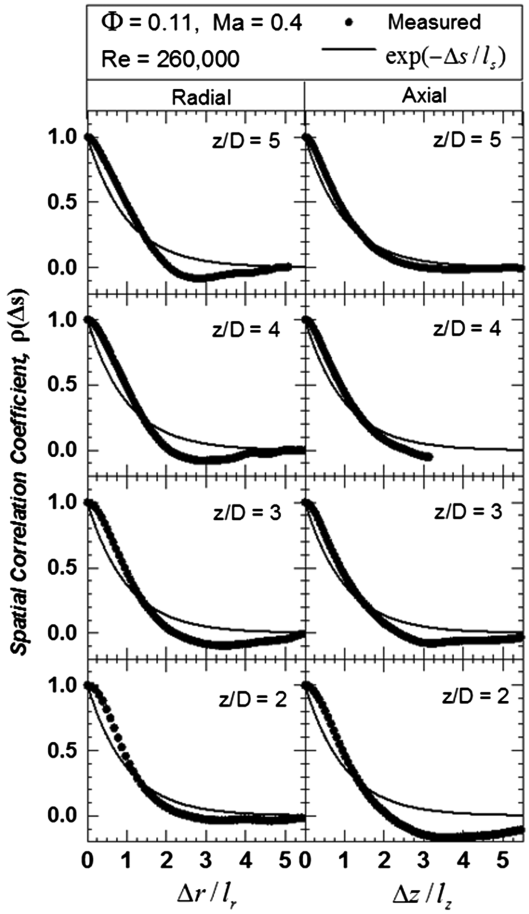

Fig. 5 Radial (left) and axial (right) spatial correlation coefficients of the radiation intensity for the exhaust plume with lowest equivalence ratio.

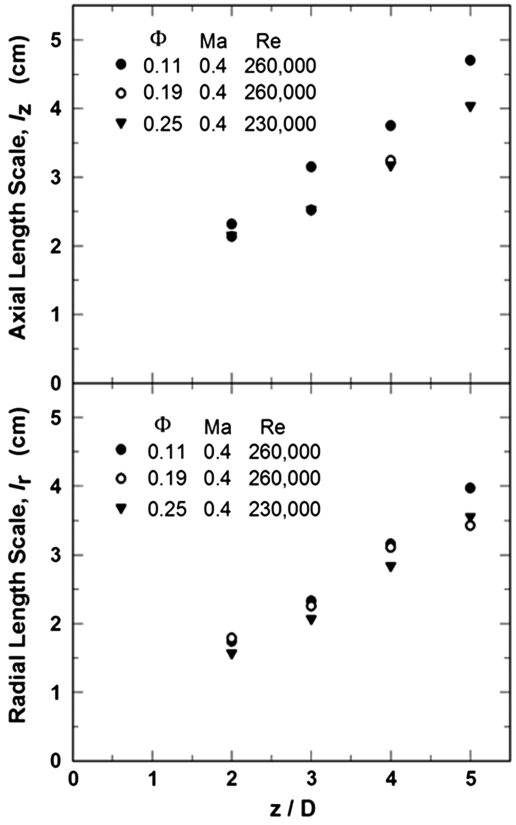

Fig. 6 Axial (top) and radial (bottom) integral length scales of the radiation intensity emitted from three exhaust plumes with varying equivalence ratios.

downstream in flames has been noted for mixture fraction measurements [11,24] and deconvoluted line-of-sight intensity measurements [15]. It is surprising that the axial integral length scales are only modestly larger (~20%) than radial length scales. Isotropic turbulence, where the two length scales would be equal, occurs downstream of this region. Ongoing work studying the radiation intensity emitted from a methane/hydrogen/nitrogen flame has indicated similar radial and axial integral length scales (within 20%) at 20 diameters downstream. The difference between the radial and axial length scales increases downstream in this flame. Further investigation is required to understand this phenomenon both in the flame and in the plumes.

Figure 7 presents the autocorrelation coefficient of the radiation intensity for the plume with the lowest equivalence ratio (0.11). Similar trends were observed for the plumes with higher equivalence ratios. The coefficient indicates the correlation between fluctuations in the intensity at 2 times at a given location. The change in time at which the correlation tends to zero indicates the maximum time between which fluctuations in the scalar values affect the path integrated intensity. The left side is plotted with respect to change in time and the right side is with the change in time normalized by the integral time scale [11]. Similar trends in the autocorrelation coefficient were observed for the plumes with higher equivalence ratios. At two diameters downstream and beyond, the autocorrelation coefficients decay rapidly to zero and then oscillate. The autocorrelation coefficients become similar when the change in time is normalized with respect to the integral time scale. This scaling is approximated reasonably well as an exponential decay. An undershooting of the autocorrelation coefficient below zero is more prevalent farther downstream in the plume (e.g., left panel, $z/D = 5$). Zheng and Gore [20] reported undershooting of autocorrelation coefficients of spectral intensity measurements of an ethylene flame. This was attributed to periodic masses of hot and cold carbon dioxide along lines of sight through the flame. This is a plausible explanation for the trend observed with the plume. Downstream in the plume

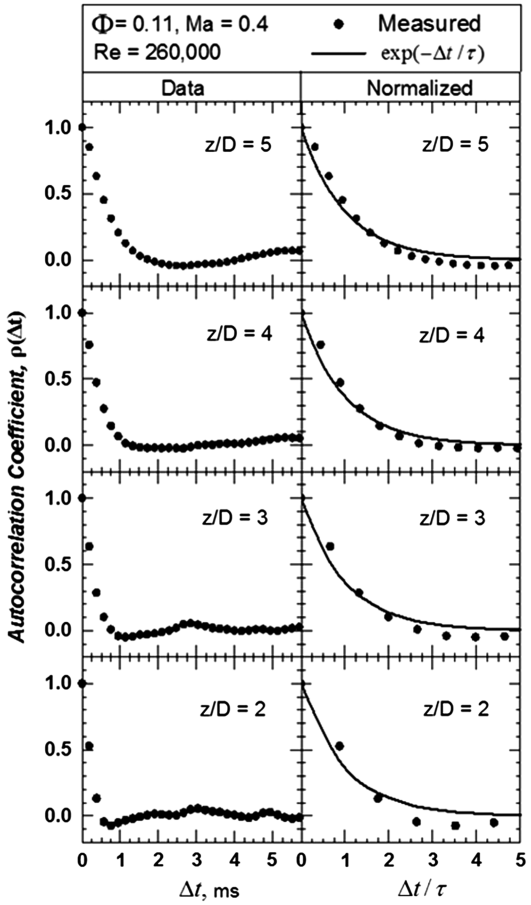

Fig. 7 Autocorrelation coefficient of radiation intensity for the plume with the lowest equivalence ratio. Panels on the left are with respect to change in time, panels on the right are with change in time normalized by the integral time scale.

intermittent regions of hot and cold carbon dioxide become more prevalent.

Integral time scales of the three plumes are shown in Fig. 8. Integral time scales indicate the time required for larger turbulent eddies to advect past a given location. The times scales in this work are path integrated as a result of the line-of-sight radiation measurements. Similar values have been used while modeling radiation emissions from turbulent partially premixed flames [15]. Integral time scales increase monotonically downstream. Similar trends have been reported in flames for local, [18], line-of-sight, [11], and deconvoluted [15] intensity measurements. The increase in the integral time scales with distance downstream is consistent with

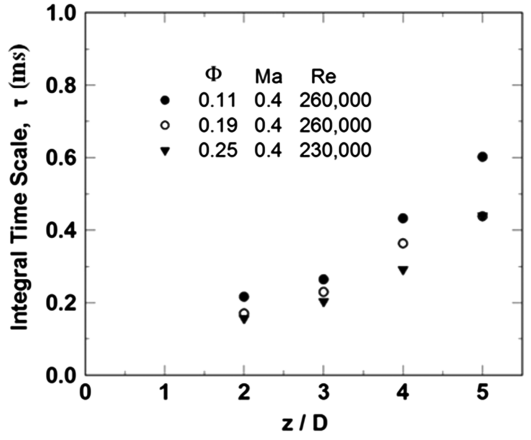

Fig. 8 Integral time scales of the radiation intensity for three exhaust plumes with varying equivalence ratios.

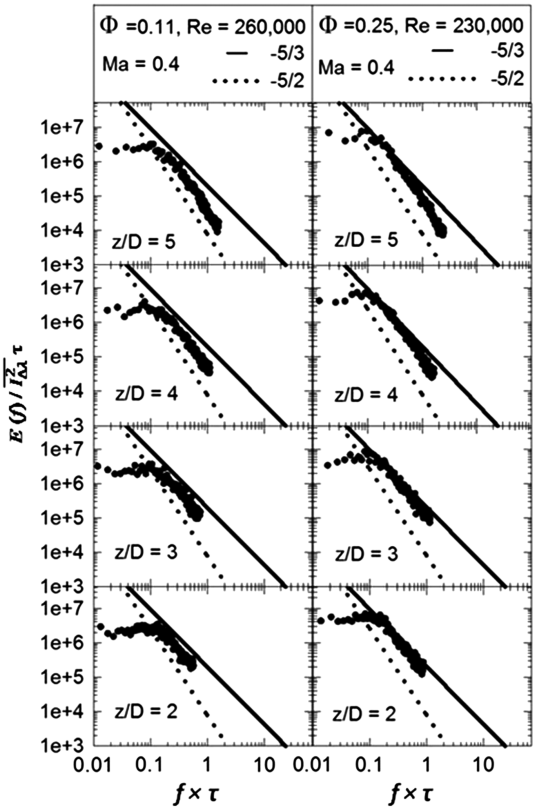

Fig. 9 Power spectral density function of the radiation intensity emitted from the plumes with the highest and lowest equivalence ratios.

Taylor's hypothesis, $\tau = l/u$ [14,16]. The axial velocity decreases downstream in the plume, while the integral length scale increases, resulting in larger integral time scales. Time scales of the present exhaust plumes are notably smaller (factor of 2–10) than corresponding values reported for jet flames with Reynolds numbers of 7400 and 12,700 [11]. The frequency of fluctuations in the intensity increases for larger Reynolds numbers. Integral time scales decrease with an increase in fluctuating frequency [23].

The power spectral density (PSD) function of the radiation intensity of paths through the centerline at four axial locations is reported in Fig. 9 for the plumes with the lowest and highest equivalence ratios (0.11 and 0.25). The PSD indicates the frequency where the inertial-like subrange of the turbulence begins. The frequency is multiplied by the integral time scale for nondimensionalization and the PSD magnitude is normalized with respect to the integral time scale and variance of the intensity [11]. This scaling allows additional frequency information to be available downstream in the plume as the integral time scale increases. The PSD profiles are similar at the various axial locations for the low and intermediate normalized frequencies. Break frequencies are between 0.1 and 0.2. Kounalakis et al. [11] reported break frequencies near 0.1 for similar measurements in carbon monoxide/hydrogen jet flames ($Re = 7,400, 12,700$). The slope of the PSD is typically $-5/3$ in the inertial-like subrange of the PSD, in agreement with that observed for the carbon monoxide/hydrogen flame [11].

Conclusions

The conclusions of this work are as follows:

1) Axial and radial variations in the normalized root mean square of the radiation intensity are similar to those reported for flames with a Reynolds number an order of magnitude smaller than that of the plumes.

2) Probability density functions of the radiation intensity become increasingly skewed toward negative values with increasing axial or radial distance as a result of intermittent emissions from the surroundings and the plume.

3) Autocorrelation coefficients of the radiation intensity downstream of the core region are approximated reasonably well by exponential decay curves. It is plausible that techniques using autocorrelation coefficients to model turbulent radiation emissions can be extended to nonreacting exhaust plumes.

4) Axial and radial correlation coefficients of the radiation intensity tend to undershoot exponential curves. This should be considered when using spatial correlation coefficients to model turbulent radiation emissions from exhaust plumes.

5) Integral time and length scales increase monotonically downstream of the core region indicating that Taylor's hypothesis is valid in exhaust plumes in this region.

6) The break frequency and slope of the normalized power spectral density function are comparable to those reported for turbulent jet flames with Reynolds numbers an order of magnitude lower than the exhaust plumes. This suggests that through proper scaling the turbulent spectra of radiation emissions have little sensitivity to the Reynolds number and the reacting or nonreacting nature of the flow.

Appendix

The mean intensity

$$I_{\Delta\lambda,\text{mean}} = \bar{I}_{\Delta\lambda} = \frac{1}{N}\sum_{i=1}^{N} I_{\Delta\lambda,i} \tag{A1}$$

is constant for stationary turbulence and is used for comparisons and calculating other turbulent statistics. Here N represents the number of measurements. The root mean square

$$I_{\Delta\lambda,\text{rms}} = \left[\frac{1}{N-1}\sum_{i=1}^{N}(I_{\Delta\lambda,i} - I_{\Delta\lambda,\text{mean}})^2\right]^{1/2} \tag{A2}$$

indicates the magnitude of the fluctuations in the radiation intensity. The probability density function

$$\text{PDF}_b = \frac{N_b}{N}, \qquad b = 1, 2, \ldots m \tag{A3}$$

is used to quantify the distribution of the fluctuations; N_b is the number of times that an intensity value falls within bin b with a width w defined as:

$$w = \frac{I_{\Delta\lambda,\max} - I_{\Delta\lambda,\min}}{m} \tag{A4}$$

where m is the number of bins [25]. Thirty bins were used in this work. Skewness toward positive or negative values in a probability density function indicates that fluctuations in the intensity tend to favor higher or lower intensity values (respectively) relative to the mean. Autocorrelation coefficients [26]

$$\rho(\Delta t) = \frac{\overline{(I_{\Delta\lambda}(t) - I_{\Delta\lambda,\text{mean}})(I_{\Delta\lambda}(t+\Delta t) - I_{\Delta\lambda,\text{mean}})}}{I^2_{\Delta\lambda,\text{rms}}} \tag{A5}$$

indicate the correlation between fluctuations in intensity at different times. Spatial correlation coefficients [11]

$$\rho(\Delta s) = \frac{\overline{(I_{\Delta\lambda}(s) - I_{\Delta\lambda,\text{mean}})(I_{\Delta\lambda}(s+\Delta s) - I_{\Delta\lambda,\text{mean}})}}{\overline{(I_{\Delta\lambda}(s) - I_{\Delta\lambda,\text{mean}})}\,\overline{(I_{\Delta\lambda}(s+\Delta s) - I_{\Delta\lambda,\text{mean}})}} \tag{A6}$$

indicate the correlation between fluctuations in the intensity at different locations; s represents both the radial and axial directions. The integral time and length scales were determined by integrating the area beneath the auto and spatial correlation curves (respectively) between the ordinate axis and where the curve crossed the abscissa axis. The power spectral density function [26]

$$E(f) = \left|\Gamma\left(\frac{(I_{\Delta\lambda}(t) - I_{\Delta\lambda,\text{mean}})}{I_{\Delta\lambda,\text{rms}}}\right)\right|^2 \tag{A7}$$

is useful for observing the frequency where the inertial-like subrange of the turbulence begins. Here Γ is the Fourier transform. The time-dependent intensity measurements were divided into 24 groups and the power spectral density function was determined for each group. The average of this processing is reported. This approach reduces the variance in the results [26].

Acknowledgments

This work was performed while the corresponding author was a graduate research assistant at Purdue University. The assistance of Benjamin Roberts in obtaining the data is greatly appreciated. Tony Tang designed the nozzle used in this work. Michael Walls of the Naval Surface Warfare Center, Crane Division, was technical supervisor for this project (contract number N00164-07-C-4725). His support is gratefully acknowledged.

References

[1] Mahulikar, S., Roa, G., Sane, S., and Marthe, A., "Aircraft Plume Infrared Signature in Nonafterburning Mode," *Journal of Thermophysics and Heat Transfer*, Vol. 19, No. 3, 2005, pp. 413–415. doi:10.2514/1.14686

[2] Banken, G., Cornette, W., and Gleason, K., "Investigation of Infrared Characteristics of Three Generic Nozzle Concepts," *AIAA/SAE/ASME 16th Joint Propulsion Conference*, AIAA Paper 1980-1160, 1980.

[3] Ajdari, E., Gutmark, E., Parr, T., Wilson, K., and Schadow, K., "Thermal Imaging of Afterburning Plumes," *Journal of Propulsion and Power*, Vol. 7, No. 6, 1991, pp. 873–878. doi:10.2514/3.23404

[4] Sugiyama, U., Adachi, K., and Tokaji, I., "Aspect-Ratio Effects on Infrared Radiation Intensity of 2-D Nozzle Exhaust Plumes," *Tenth International Symposium on Air Breathing Engines*, AIAA Paper 1991-7119, 1991, pp. 1111–1115.

[5] Heragu, S., Rao, K., and Raghunandan, B., "Prediction of Radiative Transfer from Potential Core of a Hot Jet," *Journal of Thermophysics and Heat Transfer*, Vol. 8, No. 2, 1994, pp. 368–370. doi:10.2514/3.548

[6] Decher, R., "Infrared Emission from Turbofans with High Aspect Ratio Nozzles," *Journal of Aircraft*, Vol. 18, No. 12, 1981, pp. 1025–1031. doi:10.2514/3.44742

[7] Knowles, K., and Saddington, A., "A Review of Jet Mixing Enhancement for Aircraft Propulsion Applications," *Journal of Aerospace Engineering*, Vol. 220, No. 2, 2006, pp. 103–127.

[8] Pearce, B., and Varma, A., "Radiation-Turbulence Interactions in a Tactical Missile Exhaust Plume," *AIAA 16th Thermophysics Conference*, AIAA Paper 1981-1110, 1981.

[9] Calhoon, W., and Kenzakowski, D., "Flowfield and Radiation Analysis of Missile Exhaust Plumes Using a Turbulent-Chemistry Interaction Model," *36th AIAA/ASME/SAE/ASEE Joint Propulsion Conference*, AIAA Paper 2000-3388, 2000.

[10] Blunck, D., Harvazinski, M., Gore, J., and Merkle, C., "The Influence of Turbulent Fluctuations on the Radiation Intensity Emitted from the Core Region of Exhaust Plumes," *48th AIAA Aerospace Sciences Meeting*, AIAA Paper 2010-238, 2010.

[11] Kounalakis, M., Sivathanu, Y., and Faeth, G., "Infrared Radiation Statistics of Nonluminous Turbulent Diffusion Flames," *Journal of Heat Transfer*, Vol. 113, No. 2, 1991, pp. 437–445. doi:10.1115/1.2910580

[12] Ji, J., Sivathanu, Y., and Gore, J., "Thermal Radiation Properties of Turbulent Lean Premixed Methane Air Flames," *Proceedings of the Combustion Institute*, Vol. 28, No. 1, 2000, pp. 391–398. doi:10.1016/S0082-0784(00)80235-0

[13] Kounalakis, M., Gore, J., and Faeth, G., "Turbulence/Radiation Interactions in Nonpremixed Hydrogen/Air Flames," *Proceedings of the Combustion Institute*, Vol. 22, No. 1, 1988, pp. 1281–1290.

[14] Kounalakis, M., and Gore, J., Faeth, G., "Mean and Fluctuating Radiation Properties of Nonpremixed Turbulent Carbon Monoxide/Air Flames," *Journal of Heat Transfer*, Vol. 111, No. 4, 1989, pp. 1021–1030. doi:10.1115/1.3250763

[15] Zheng, Y., Barlow, R., and Gore, J., "Spectral Radiation Properties of Partially Premixed Turbulent Flames," *Journal of Heat Transfer*, Vol. 125, No. 6, 2003, pp. 1065–1073. doi:10.1115/1.1621902

[16] Zheng, Y., Sivathanu, Y., and Gore, J., "Measurements and Stochastic Time and Series Simulations of Spectral Radiation in a Turbulent

Non-Premixed Flame," *Proceedings of the Combustion Institute*, Vol. 29, No. 2, 2002, pp. 1957–1963. doi:10.1016/S1540-7489(02)80238-3

[17] Silva, C., Malico, I., and Coelho, P., "Radiation Statistics in Homogenous Isotropic Turbulence," *New Journal of Physics*, Vol. 11, No. 9, 2009, p. 093001. doi:10.1088/1367-2630/11/9/093001

[18] Dylla, J., Sivathanu, Y., and Gore, J., "Multivariate Spatial Correlation Measurements in Turbulent Jet Flames," *31st AIAA Aerospace Sciences Meeting*, AIAA Paper 1993-0801, 1993.

[19] Biswas, K., Zheng, Y., Kim, C., and Gore, J., "Stochastic Time Series Analysis of Pulsating Buoyant Pool Fires," *Proceedings of the Combustion Institute*, Vol. 31, No. 2, 2007, pp. 2581–2588. doi:10.1016/j.proci.2006.07.234

[20] Zheng, Y., and Gore, J., "Measurements and Inverse Calculations of Spectral Radiation Intensities of a Turbulent Ethylene/Air Jet Flame," *Proceedings of the Combustion Institute*, Vol. 30, No. 1, 2005, pp. 727–734. doi:10.1016/j.proci.2004.08.255

[21] Blunck D., and Gore, J., "A Study of Narrowband Radiation Intensity Measurements from Subsonic Exhaust Plumes," *Journal of Propulsion and Power*, Vol. 27, No. 1, 2011, pp. 227–235. doi:10.2514/1.47962

[22] Moffat, R., "Describing the Uncertainties in Experimental Results," *Experimental Thermal and Fluid Science*, Vol. 1, No. 1, 1988, pp. 3–7. doi:10.1016/0894-1777(88)90043-X

[23] Karpetis, A., and Barlow, R., "Measurements of Scalar Dissipation in a Turbulent Piloted Methane/Air Jet Flame," *Proceedings of the Combustion Institute*, Vol. 29, No. 2, 2002, pp. 1929–1935. doi:10.1016/S1540-7489(02)80234-6

[24] Pope, S., *Turbulent Flows*, Cambridge Univ. Press, Cambridge, England, U.K., 2005, p. 69.

[25] Bendat, J., and Piersol, A., *Random Data: Analysis and Measurement Procedures*, Wiley, New York, 2010.

[26] Zheng, Y., *Spectral and Total Radiation Properties of Turbulent Non-Luminous Jet Flames*, Ph.D. Thesis, Purdue Univ., West Lafayette, IN, 2003.